Mechanistic Study of the Interplay of Intestinal Transport and Metabolism Using the Synthetic Modeling Method

Yu Liu[1] and C. Anthony Hunt[1, 2]

[1] The UCSF/UCB Joint Graduate Group in Bioengineering, University of California, Berkeley, CA, USA
[2] The Department of Biopharmaceutical Sciences, Biosystems Group, University of California, San Francisco, CA, USA

Corresponding Author:
C. Anthony Hunt
Department of Biopharmaceutical Sciences
513 Parnassus Ave., S-926
University of California
San Francisco, CA 94143-0446
P: 415-476-2455
F: 415-514-2008
E: hunt@itsa.ucsf.edu

ABSTRACT

Purpose. Demonstrate the feasibility of a new class of experimental computational models built using the synthetic method. Study the consequences of spatial alignment, or lack thereof, of Pgp and CYP3A4 on the transport and metabolism of drug-like compounds and the influence of competitive inhibition by metabolites on the transport and metabolism of those compounds.
Methods. The synthetic method of modeling and simulation was used to construct discrete event, discrete space models. Within a framework designed for experimentation, object-oriented software components were assembled into devices representing the efflux transport and metabolism mechanisms within cell monolayers in Caco-2 transwell systems.
Results. Conditions for transport and metabolism synergism (and lack thereof) were identified. Simulations showed how spatial alignment altered the coordinated influences of Pgp and CYP3A4 on absorption of a series of drug-like compounds. Within those experiments, when the metabolites were also substrates of Pgp, the metabolite levels produced were insufficient to give evidence of a competitive inhibitory effect on either transport or metabolism.
Conclusions. The results provide convincing support for the feasibility of using this new class of models to improve our understanding of how complex cellular processes influence the transport and absorption of compounds, and the consequences of interventions.

KEY WORDS: Drug absorption; agent-based modeling; simulation; P-glycoprotein; CYP3A4.

INTRODUCTION

By improving our understanding of how the intra- and intercellular processes within the small intestine collectively act to influence the transport of compounds, our ability to make predictions more reliable and to anticipate the consequences of interventions will also improve (1). One of the best ways to understand how a complex system functions is to build a functioning analog of that system that exhibits some of the phenomena of interest. Many *in vitro* and *in situ* models used to study drug metabolism are intended to do that. However, all of the complexity of these model systems resides in their living parts, and using biotechnological methods (that start with inert components) to construct analogs of those living parts will remain infeasible for the near future. The traditional approach continues to be to study and experiment on those *in vitro* and *in situ* models, as well as the referent organisms, and then to induce mechanistic explanations that adequately account for the patterns observed in collected transport and absorption data. The more useful and predictive explanations have typically been based on sets of differential equations. The equations provide abstract descriptions of the behavior of the hypothesized mechanisms under the conditions specified. Examples are discussed by Grass (2).

We report on a new computational approach to augment the traditional approach. In silico components, built using object-oriented programming, are used to construct and synthesize working devices that implement hypothesized mechanisms. The components can be made to realistically represent biological counterparts, as needed, at a level of detail appropriate for the available knowledge and data. Our goal is to build synthetic, in silico models of the intestine and connected tissues that are suitable for studying the mechanisms, conditions, and interventions hypothesized to influence drug absorption. We recently described models that mimic aspects of confluent Caco-2 cells growing in a transwell system (3). The models are transparent and intuitive, and all of the components map logically to cellular and transwell system counterparts. We reported results of experiments that verified the key model design features, including the ability to reliably represent passive paracellular and transcellular transport, carrier-mediated transport, and active efflux transport for simulated compounds having a wide range of physicochemical properties. In addition, specifically parameterized devices generated acceptable matches to reported *in vitro* transport data for alfentanil and digoxin. We have used the same

type of devices for the studies described herein. They are intended to function as in silico analogs of transwell systems containing a layer of epithelial cells; hereafter we refer to such a device as an in silico transwell system (ISTS).

We now aim to demonstrate the feasibility of using ISTSs to help study how the mechanisms of transport, efflux, and metabolism interact through common substrates to influence the transport and metabolism of drug-like compounds. We also want to identify system specifications that give rise to efflux-metabolism synergy and those that do not. We add to the case for feasibility by showing that ISTSs can be used to test hypotheses about how the interplay between an efflux transporter, such as P-glycoprotein (Pgp), and a Phase I metabolic enzyme, such as CYP3A4, is believed to influence the intestinal absorption of drug-like compounds (4). The software components used to represent transporters and metabolic enzymes are generic. Hereafter, Pgp and CYP3A4, the most documented pair, is the example studied.

It has been proposed that Pgp and CYP3A4 might act as a coordinated molecular barrier to drug intestinal absorption because of the significant overlap of their substrate specificities (5). The fact that they co-localize near the apical side of enterocytes and can be co-induced and co-inhibited by many compounds (6), has led some to suggest that Pgp and CYP3A4 synergy helps reduce the absorption of dual substrate compounds (7, 8). The increased absorption caused by inhibition of both Pgp and CYP3A4 is taken as evidence of that synergism.

Because it is inherently difficult to represent spatially localized phenomena in an equation-based model, no traditional models have been proposed to study the consequences of Pgp and CYP3A4 being spatially aligned. However, Ito et al. (9), using a compartment pharmacokinetic model, has shown that the fraction absorbed is synergistically elevated by simultaneous inhibition of both Pgp and CYP3A4. If one could control the relative intracellular location of Pgp and CYP3A4 within Caco-2 or the other cell lines, then it would be possible to experimentally measure the importance of spatial alignment, but such technology is not available. Computationally, it is easy to control the location of counterparts of Pgp and CYP3A4 within an ISTS and thereby examine the consequences of their spatial alignment. We speculated that alignment may be just one of several factors interacting to influence synergy. It seemed clear that spatial alignment of Pgp and CYP3A4 would cause synergy for a dual substrate compound. The degree of synergism when Pgp and CYP3A4 locations are uncorrelated under the same conditions was, however, unclear, and so merited study. We hypothesized that, when locations are uncorrelated, the contribution of Pgp–CYP3A4 synergism to the transport properties of dual substrate compounds would be influenced by the density of Pgp and CYP3A4, as well as by the relative, Pgp-compound and CYP3A4-compound affinities.

It has been proposed that Pgp can also enhance intestinal drug metabolism by facilitating the removal of metabolites, thereby preventing competitive inhibition of the enzyme by its metabolite (10). However, there are two reasons why Pgp-mediated efflux cannot be generalized to all CYP3A4 metabolites. First, some metabolites do not show selective efflux to the apical side of epithelial monolayers. Second, some of the preferential apical distribution that has been observed is not changed by Pgp's inhibition (11, 12). Consider the case where metabolites of CYP3A4 are also Pgp's substrates and they can interact with CYP3A4, thus inhibiting drug access. If drug efflux is being competitively blocked by the already existing metabolites, will there be altered metabolism of the parent drug? To date, it has been difficult to address such questions in wetlab experiments, in part because the available compounds (and their metabolites) often do not have the required combination of properties. With the technology described herein, it is now also possible to address such questions using in silico experimentation. Within an ISTS we can control the affinities of each in silico metabolite for simulated Pgp and CYP3A4 components. Toward this aim, two sets of identical in silico compounds were created: all the metabolites of the first set are substrates for the simulated Pgp, whereas none of the metabolites in the second set are substrates. The expectation was that if the competitive inhibitory effect on either efflux or

metabolism is significant under the conditions of our experiments, then there will be evident differences in the overall transport properties of the two sets.

The results of our in silico experiments verify that ISTSs do generate transport and metabolism behaviors similar to those observed in the experiments using the *in vitro* CYP3A4-transfected Caco-2 transwell system for single and dual substrate compounds. The separate and combined simulated influences of Pgp and CYP3A4 on the in silico transport of 17 virtual compounds have been systematically documented. We have used that data to explore two mechanistic questions and tested the related hypotheses. Correlated spatial alignment had a unique effect on the coordinated influences of simulated Pgp and CYP3A4 on simulated absorption. However, for the ISTSs described, there was no evidence of a competitive inhibitory effect on either transport or metabolism from the simulated metabolites that were substrates of simulated Pgp. Taken together the results provide convincing support for the feasibility of developing and using synthetic models to improve our understanding of how the complexity of cellular processes influences absorption. Further experimentation with ISTSs is expected to provide improved insights and specifically suggest targeted experiments to challenge new insights.

METHODS

Model Structure, Design, and Assumptions

The structure of the ISTS is illustrated in Fig. 1 and detailed by Liu and Hunt (3). It mimics essential features of a CYP3A4-transfected Caco-2 cell monolayer in a cell culture transwell system (13). The ISTS represents an arbitrary width, vertical column section through the entire transwell system. This section is sliced virtually into five stacked segments. Each segment is represented by a discrete 2D space (e.g., a 100 x 100 grid). The components of interest within the five spaces—compounds, cells, enzymes, metabolites, etc.—are represented as objects. All processes are represented by a set of discrete-event driven behavioral causality relations. Each process in the ISTS represents a known or hypothesized biological mechanism. Discrete time steps are used to represent continuous time. When used within an appropriate simulation framework, the resulting software devices can operate in ways that represent the hypothesized biological mechanisms within epithelial monolayers, at the level of detail and resolution needed to meet a particular research objective. We therefore refer to them as being biomimetic. The resulting devices are examples of a class of object-oriented, hierarchical, modular simulation models that are being developed within other scientific and technical domains (14, 15). Several distinctions are provided in the Discussion section between this class of models and traditional equation-based models.

Grid dimensions and the width and depth of the vertical column in Fig. 1 all control the system resolution. New spaces can be added by plugging in new grids without having to reengineer the model. *G1* represents a portion of the apical lumen compartment and the fluid in the transwell insert. *G2* represents the apical membranes of the cell monolayer and the junctions between cells viewed from the apical side. *G3* represents the intracellular spaces. *G4* represents the basolateral membranes and the junctions between cells viewed from the basolateral side. Within *G2* and *G4*, a parameter controls the prevalence of simulated tight junctions between cells. A percentage of grid points in each of these two spaces are chosen randomly to represent junctions; the remaining grid space represents cell membranes. *G5* represents a portion of the basolateral compartment and the fluid in the cell culture well. These spaces accommodate other system components.

[Figure 1]

Differently parameterized ISTSs are used and measured during in silico experiments in the same way as a Caco-2 monolayer within a biological transwell system. The ISTS framework is built of modular components using the Java layer of the Swarm platform (16). Within the computational framework, we have an agent, the *Experiment Agent*, to manage experiments. It is the in silico counterpart to the researcher conducting wetlab experiments. When needed, a *Data Model* can be used to hold data from *in vitro* experiments. A *Reference Model* can be one of the existing mathematical models (e.g., a pharmacokinetic model in Ito et al. (9)) that are used to represent drug transport through cell monolayers or the small intestine. The *Experiment Agent* reads inputs from the *Parameter Manager* and transfers that information to the ISTS. Simulation results are collected in the *Data Management Module* for statistical processing.

System Components

To avoid confusion and clearly distinguish *in vitro* components and features from corresponding in silico components and features, such as a "cell," a "drug," or "metabolism," we use SMALL CAPS when referring to the in silico components. A mobile object called DRUG represents actual drug molecules. Seventeen different DRUGS were used; their properties are listed in Table I. A typical DRUG represents more than one molecule and can move within and among spaces. Movement of a free DRUG to an adjacent, less-crowded location within a grid is governed by a biased random walk (3). Its traverse from one space to another is governed by its location, its assigned physicochemical properties (here we consider only lipophilicity, degree of ionization, and molecular size), and environmental conditions, including the concentration gradient, pH, etc. Molecular weight (MW) is used to determine the in silico diffusion coefficient (D_{ISTS}): $D_{ISTS} \propto 1/(\mathrm{MW})^n$. We assume $n = 1$ in the BILAYER (*G2* and *G4*) and 0.6 elsewhere (17, 18). Entering the BILAYER from an aqueous space is controlled by an event probability that is influenced by the above factors. The probability of exiting that space at the next time step is arbitrarily set to 0.5.

[Table I]

Membrane transporters and metabolic enzymes are modeled as immobile objects. Objects called PGP represent Pgp. Objects called CYP represent CYP3A4, the only metabolic enzyme considered in this study. Both PGP and CYP can be assigned randomly or to specific locations within the *G2* and *G3* spaces, respectively. Each can only interact with a DRUG located at its active site. The number of PGP and CYP can be specified separately in advance or drawn separately at random from a uniform distribution having specified minimum and maximum values. PGP is only parameterized to transport DRUG out of the simulated cell interior to *G1*. Because there may be several transporters within the area of cell membrane represented by one *G2* location, each PGP may represent more than one transporter. Both PGP and CYP have a free state and three occupied states, as diagrammed in Fig. 2. If a DRUG is located adjacently to the active site of a free PGP or CYP, binding can occur with a probability that depends on the value of their solute affinity parameters (*cyp-* and *pgpSoluteAffinity* in Table I). Those parameter values, together with the reactivity of the complexes, are conflated in silico into the probability of DRUG binding. A larger parameter value corresponds to a smaller value of K_m in Michaelis-Menten models (3). An occupied PGP holds its DRUG for three time steps, corresponding to the illustrated state changes in Fig. 2, and then releases it into the simulated apical space, *G1*. In simulations of intracellular metabolism, three time steps after a DRUG is bound to CYP, its METABOLITE is placed in a location adjacent to the now free CYP. Thereafter, the METABOLITE randomly moves within and among spaces, exactly as would its parent. For simplicity, METABOLITES are given the same physicochemical properties as their parents. However, when it is required, it is easy to change parameters to individualize METABOLITE properties. For example, in one experiment the METABOLITE can have the same PGP and CYP affinity values as the parent. In another, those

values can be set to zero. Additional objects representing networks that control the level of expression of enzymes and transporters, or other cellular components such as other transporters, lysosomes, and genes, can be specified and added when needed.

For each stochastic event, a random number is drawn from a standard uniform distribution and compared with a pre-specified or calculated event probability. Events occur only when the random number is less than or equal to the parameterized event probability.

[Figure 2]

In Silico Experiments and Data Analysis

In all experiments, the pH in *G1*, *G3,* and *G5* is equal to 7.4. At the start of a simulation 2,000 DRUG objects are assigned to random locations in the donor space. Because of the stochastic nature of events within the same simulation, repeated measurements of a behavior of interest will differ between experiments (between model runs). However, for repeat Monte Carlo simulations (e.g. 50), the behaviors discussed herein have reasonably symmetric frequency distributions; the central limit theorem is applicable.

In Table II the ISTS parameters are grouped into three categories: 1) the simulated transwell system; 2) the physicochemical and biochemical properties assigned to DRUGS; and 3) the in silico experimental conditions. An ISTS is designed to study and document DRUG transport from either direction. When *G1* is designated as the donor compartment, apical-to-basolateral (A→B) transport is simulated. When *G5* is designated as the donor compartment, B→A transport is simulated. Experiments are run for a certain period under a sink condition; e.g. for studies in which only initial flux rates were measured, the period is when no more than 10% of of the dose has transported from the donor to the receiver space. The initial flux rates are calculated by dividing the amount of DRUGS in the receiving space by elapsed time steps (dQ/ds). The in silico apparent permeation coefficient is $P_{ISTS} = (dQ/ds)/(a \times c_0)$, where a is the area of the first membrane space contacted (*G2* or *G4*), and c_0 is the initial dose of DRUGS. Extraction ratio (ER), which is a measurement of the extent of metabolism relative to the amount of transported drugs, is calculated as in Cummins et al. (19):

$$ER = \sum METABOLITES_{all\ grids} / (\sum METABOLITES_{all\ grids} + \sum Parents_{G2,3,4\&5}).$$

[Table II]

PGP and CYP interact only with DRUGS or METABOLITES that they recognize as being substrates. Each DRUG or METABOLITE carries a label that designates it as a substrate or not. To inhibit the interaction of PGP or CYP with a substrate, that label recognition is blocked for the duration of the study; the result is complete inhibition. By changing PGP and CYP densities, their binding affinities for the DRUG (and METABOLITE) under study, and/or each DRUG's corresponding physicochemical properties, we are able to study the combined influences of efflux and METABOLISM for a wide variety of simulated compounds.

RESULTS

The Influence of PGP and CYP on Single Substrate DRUGS

The passive transport behaviors of DRUG **I** have been described in detail (3); **I** served as the control in this study. To study the influence of PGP alone, we made two virtual analogs—**II** and **III**—that are exclusive substrates of PGP, having *pgpSoluteAffinity* values of 0.5 and 0.75, respectively. The ISTS contained 10 or 30 PGPs in *G2*. Because **I** is not a PGP substrate, it did not exhibit any significant difference between A→B and B→A transport. For **II** and **III**, their B→A transport always exceeded that of A→B because of the added influence of unidirectional efflux driven by PGP (Fig. 3A). The magnitude of the effect increased as both PGP-DRUG affinity and PGP density in *G2* increased. At time step 400, the highest intracellular DRUG levels were observed for **I**, and were indistinguishable for both transport directions (Fig. 3B). When efflux was involved, the intracellular levels decreased for both transport directions, indicating the pivotal role of active efflux in maintaining lower intracellular levels of substrates.

To study the influence of CYP alone, two new analogs of **I** were created. As listed in Table I, **V** and **IX** have *cypSoluteAffinity* values of 0.5 and 0.75, respectively, but no PGP affinity. The A→B transport simulations were conducted in an ISTS limited to only 20 or 50 CYPS in *G3* and were run for 400 time steps. **I**, which was not recognized by CYP, exhibited more transport and had the highest intracellular DRUG levels. As CYP-DRUG affinity and the number of CYP increased, fewer DRUGS were transported to *G5*, and a significant decrease in intracellular DRUG levels was observed (Fig. 4A). Extraction ratio (ER) values increased as CYP-DRUG affinity and/or the number of CYP increased, because of increased METABOLISM and decreased transport to the *G3* and receiver spaces (Fig. 4B). Together the data show, as expected, that metabolism reduced DRUG transport and intracellular DRUG levels.

[Figure 3 and 4]

The Influence of PGP and CYP on Dual Substrate DRUGS

To study the combined influence of PGP and CYP on transport behavior, we used **VI**, **VIII**, **XIV**, and **XVII**. Each is a dual substrate having the properties listed in Table I. Each ISTS contained 20 CYPS and 30 PGPS. To isolate the consequences of PGP and CYP inhibition, A→B and B→A control studies were conducted for all four DRUGS. Protocols were repeated to study three different treatments: complete inhibition of PGP, complete inhibition of CYP, and complete inhibition of both. All other factors and parameter values were kept constant.

VI and **XVII** have identical PGP and CYP affinities, but different physicochemical properties. Net B→A transport exceeded A→B transport for both DRUGS, but as seen in Fig. 5A and 5C, the difference is more apparent for **XVII** because of its physicochemical properties. This polarized transport was completely abolished by inhibition of PGP: the result was decreased B→A and increased A→B transport relative to the control values. When PGP and CYP were both inhibited, A→B transport increased even further due to the additional effect of blocked METABOLISM. The simulated intracellular and basolateral levels of the two DRUGS at time step 400 (for **VI**) or 1,000 (for **XVII**) were significantly increased relative to the control values (Fig. 5B and 5D). Because of the increased *G3* DRUG levels caused by PGP inhibition, the levels of total METABOLITES also increased. The *G3* levels, but not the *G5* levels of the two DRUGS, were affected by CYP inhibition.

[Figures 5]

Table III lists the efflux ratios for **VI** and **XVII** along with corresponding values for **VIII** and **XIV**. The data show how much ER values changed due to PGP inhibition. Compared to **VI**, **XVII** had a larger efflux ratio because of its physicochemical properties. **VIII** had a larger efflux ratio due to its stronger interaction with PGP. Inhibition of PGP decreased the ER of all four DRUGS. **XVII** had the largest decrease (14.3%) and **VI** had the smallest (3.5%). **XIV** had a greater affinity for CYP than did **VI**, and yet they had the same PGP-DRUG affinity and physicochemical properties. Consequently, they had a similar efflux ratio. However, inhibition of PGP decreased the ER of **XIV** (11%) more than it did the ER of **VI** (3.5%).

[Table III]

Synergism may occur between PGP and CYP in retarding the ABSORPTION of the dual substrate DRUGS studied. Synergism is confirmed when the additional amount ABSORBED when both PGP and CYP are inhibited, relative to control values (no inhibition), is greater than the sum of additional amounts ABSORBED after separately inhibiting PGP and CYP. We made such measurements for several of the experiments described above after 400 and 800 time steps. In most cases, when the numbers of PGP and CYP were low (e.g., 30 and 20 each or less) there was no evidence of synergism with a short absorption interval. For larger densities of PGP and CYP (e.g., 50 each) and longer study intervals, clear evidence of synergism was obtained for the dual substrates in Table I. Results for **VI** and **XI** are shown in Table IV.

[Table IV]

Studies of PGP and CYP Relative Location

To test our first hypothesis, we constructed two different groups of ISTSs, one control, and the other experimental. We used each to conduct experiments on **I–XVI.** We specified that each ISTS contain 50 PGPS and 50 CYPS. In the control ISTSs, the PGPS and CYPS were randomly assigned to locations within their corresponding spaces, *G2* and *G3* respectively, so that there was no correlation between their relative locations. For the experimental ISTSs, the PGPS (or CYPS) were first randomly assigned to locations in their space, and their grid coordinates were recorded. Next, the CYPS (or PGPS) were placed at matching coordinates within their space. Viewed from *G1* each PGP is "above" a CYP.

The influences of the relative positioning of PGP and CYP on measured flux rates and ER values are shown in Fig. 6 and 7, respectively. The data are grouped by CYP-DRUG affinity value, and within each set there are mean data for four different PGP-DRUG affinity values. For the dual substrates, matched PGP-CYP positioning had no significant effect on B→A flux rates, but it did have a modest but significant effect on A→B flux rates (Fig. 6). For the PGP substrates the B→A flux rates were clearly larger than those for A→B, and the magnitude of the difference increased with increasing PGP-DRUG affinity. For the dual substrates, there was a clear influence of PGP-CYP relative positioning on measured ER values (Fig. 7) for each of the A→B experiments. That influence was less dramatic for the B→A experiments. In fact, for **X**, **XIV** and **XV**, differences between experimental and control B→A experiments were not statistically significant. With increasing PGP-DRUG affinity, ER decreased in B→A transport for both control and experimental groups. ER values for A→B transport were different. ER increased within the control group, but decreased within the experimental group. In other words, for dual substrate DRUGS in an ISTS where the locations of PGP and CYP are spatially aligned, inhibition of PGP increased ER for both B→A and A→B transport. It is noteworthy that no *in vitro* experiments have reported such a phenomena.

[Figures 6 and 7]

Studies of Competitive Inhibition by METABOLITES

To test our second hypothesis, we conducted two sets of experiments. Both used **I–XVI** and ISTSs having independent, random placement of PGP and CYP. Within each set, each METABOLITE was assumed to have the same CYP affinity as its parent. For the first set of experiments METABOLITE affinity for PGP was identical to that of its parent. For the second set of experiments PGP-METABOLITE affinity was zero. For A→B and B→A simulations we compared the consequences of the two mechanisms on initial flux rate measures and ER values. We used analysis of variance (ANOVA) to test if there was a statistically significant difference between the two mechanisms. If so, it would indicate that within the first set of experiments, there was evidence of competitive inhibition being a significant factor.

Tables V and VI display the results of the ANOVA analysis. The differences between DRUGS are sufficient to account for all of the variance in initial flux rates and ER values for both A→B and B→A transport (p-values for the DRUG term ≈ 0). There was no statistically significant evidence for a contribution from either of the two mechanisms. Nor was there any significant evidence for a contribution from the interaction term (a specific combination between DRUG and one of the mechanisms). For the conditions studied there was no experimental evidence of interference through any form of competitive inhibition by METABOLITES with the transport behaviors of the parent drug. To obtain evidence of competitive inhibition by METABOLITES, more extreme conditions and properties will be required.

[Table V]

[Table VI]

DISCUSSION

Most of the models used in pharmaceutical research fall into three broad categories: constructed synthetic wetlab models, induced equation-based models, and statistical models. Here we are concerned with the first two. *In vitro* wetlab models are the mainstay of biomedical research. They are synthetic models where some of the building blocks are laboratory items and others are living parts. The Caco-2 transwell system is an example. Equation-based models are typically arrived at using the inductive method of modeling (20). They are usually built by analyzing data, creating a mapping between the envisioned structure of the system and components of the data, and then representing those data components with mathematical equations. These equations are then executed and validated against the data. Validation often involves fitting the equations to the data. Examples include simple Michaelis-Menten models, oral drug absorption models (2), and physiologically based toxicokinetic models (21). This modeling method stays very close to the data and, when successful, provides models that extrapolate beyond the original data, making them usable for prediction. However, the detail that is abstracted away when an equation is induced is where much of the heuristic value lies. That detail describes the mechanism by which the data were generated, whereas the mathematics only describes the abstracted properties of the mechanisms that are reflected in the data. To address questions about those details and how they influence system behavior we need to have a model that can include more detail, an analog of hypothesized or plausible mechanisms. To do that in silico we need to follow the synthetic modeling method (20).

There is a huge gap between experimental wetlab models and traditional computational models. The gap sits on the continuum between experiment and theory. To develop exploitable insight into the functioning of complex biological systems we need to begin bridging this gap. To do that, we need new methods beyond those described by Noble (22) and Kitano (23). From these new methods will come new classes of models that make computational biology more experimental and wetlab research more computational. The ISTSs described herein are examples of new methods to help narrow that gap. They are discrete event, discrete space, discrete time

models (14, 15) in which object-oriented software components are plugged together and operated in ways that represent the mechanisms that are believed to influence transport across the intestine and across the cell monolayer within transwell systems. The results presented above show that ISTSs can be used to experimentally explore mechanistic questions and hypotheses involving the overlapping substrate specificities of CYP3A4 and Pgp. Such issues can be challenging to address using the available *in vitro* models, and difficult to untangle from data using traditional equation-based models.

For compounds that are dual substrates of CYP3A4 and Pgp, *in vitro* experiments have shown that pretreatment with Pgp inhibitors results in a reduction in ER values (24, 25). The explanations have focused on intracellular drug levels. For example, absent Pgp inhibition, efflux of drug followed by reabsorption effectively prolongs the intracellular access of drug to the metabolizing enzymes. Pgp inhibition then blocks that prolonged access causing reduced ER values. We tested that idea and others by exploring PGP–DRUG–CYP interactions in detail. The results were similar to those observed *in vitro* (25-28). We measured the transport of dual substrates while inhibiting PGP. Relative to control values, total METABOLITES increased, as did the levels of DRUGS in CELLS and in the receiver (*G5*). ER values decreased because the *G3* and *G5* DRUG levels increased more relative to those of total METABOLITES. For example, in Figure 5D, by inhibiting PGP, the sum of the *G2*, *G3*, *G4* and *G5* levels of **XVII** increased from 109.9 to 158.4 (a 44% increase); the total amount of metabolites went from 39.7 to 48.7 (a 23% increase). Consequently, ER values decreased 12%, from 0.266 to 0.235. In the absence of PGP inhibition, the lower *G3* DRUG level caused fewer METABOLITES to be formed. However, because the net amount of DRUG transported into CELLS and to the receiver was even lower, the calculated ER seemed large. Inhibiting PGP decreased the ratio of total METABOLITES to the amount of transported DRUG, thus decreasing ER. Exploratory ISTS simulation helps bring clarity to such relationships.

We used ISTSs to explore the consequences of aligning, or not, the spatial locations of PGP and CYP within their respective spaces relative to the direction of transport. The *in vitro* experimental results are consistent with an unaligned, uncorrelated spatial arrangement, not with spatial alignment. In the in silico A→B experiments that used dual substrates, METABOLISM and efflux decreased the probability that a DRUG would arrive in the receiver space within some interval. When PGP and CYP were aligned in their respective X-Y planes, interaction with one effectively impeded interaction with the other. Consequently, their combined barrier effect was decreased relative to what it would have been with any other spatial arrangement. When a DRUG was pumped out of the CELL to *G1*, it could diffuse around within *G1* before moving back into *G3*. When PGP and CYP were aligned, it was unlikely that a DRUG would re-enter *G3* close to its exit site immediately after being pumped out. That likelihood would decrease further if we had simulated rapid mixing or transit in *G1*. The effective role of PGP in the spatial alignment case was to move DRUGS away from the site of METABOLISM, thus decreasing ER. For B→A, only metabolism decreased DRUG transport to the receiver space. Alignment, or lack thereof, had no effect on flux rate. There was, however, an alignment effect on B→A ER values when CYP-DRUG affinity was comparable to, or relatively smaller than, that for PGP-DRUG (**VI**, **VII**, **VIII**, **XI**, **XII**, **XVI**). A higher PGP affinity caused DRUGS to be pumped out of the CELLS before they could be metabolized. Those DRUGS had a lower ER than their counterparts in the control group, for which there was no alignment.

We did not find any statistically significant evidence of competitive inhibitory effects by METABOLITES on DRUGS' transport and METABOLISM. The interaction of PGP with any substrate used here can be described using simple Michaelis-Menten kinetics (3). Consequently, for METABOLITES that are Pgp substrates, inhibition will occur when METABOLITE levels are large enough. That turned out not to be the case here. The occasional inhibition that did occur was insignificant. ER was a contributing factor; those values tended to be small (< 0.5) for all

studies. Furthermore, because all experiments were conducted under sink conditions, the number of METABOLITES formed was always small relative to the initial amount of DRUG. More extreme conditions will be needed to explore METABOLITE inhibition.

Because of the synthetic nature of ISTSs, it was relatively easy, using selective inhibition of dual substrate DRUGS, to directly measure the separate and combined influences of PGP and CYP on the fraction of DRUG absorbed (transported). We observed that by so doing we could get a direct measure of synergism, which can be difficult to obtain directly form some other types of models, including *in vitro* systems. Table IV lists two cases where significant synergism was observed. More synergy can be observed given an ISTS with relatively high densities of PGP and CYP, substrates that have larger DRUG-PROTEIN affinities, and a longer duration of the experiment (data not shown).

One of our goals is to create extensible, validated ISTSs that are suitable for experimentation. We anticipate that such devices will be useful for exploring and addressing mechanistic questions and hypotheses that are difficult or impossible to address using either traditional wetlab or mathematical modeling methods. To achieve that objective the devices and their components need to be modular, as are the current ISTSs. They are purposefully abstract. Only those cellular components, features, and functions that were deemed essential to demonstrate feasibility or to address the questions of interest were included. Having demonstrated feasibility, we can then focus on a broad array of model uses and on iteratively improving these devices so that they become more reliable and useful research analogs of transwell and other systems.

ISTSs will be helpful in solving scientific problems related to transport and metabolism *in vitro*. For example, Mouly et al. (25) observed that more of a metabolite of Saquinavir (referred to as M7), the first of the HIV protease inhibitors to reach the market, was produced after basolateral dosing, than after apical dosing in a transwell system. They offer several plausible explanations. Given the modular nature of ISTSs, it is relatively straightforward to add alternative plausible mechanisms into different ISTSs that are constructed and parameterized to represent Saquinavir transport and metabolism. By so doing one can conduct experiments to contrast the influences of the different mechanisms on B→A and A→B METABOLISM. As a consequence of this competition between alternative mechanisms, one or more will survive based on their ability to generate data that is most similar to the referent *in vitro* data. This will allow for the design of targeted *in vitro* experiments to test the selected mechanisms.

To achieve the above vision it will be necessary to flexibly adjust the amount of cellular functionality and detail that an ISTS can represent. Ideally, such detail will be added only when it is needed to account for specific *in vitro* observations. Here are three examples. Additional spaces may be needed between *G1* and *G2* to represent an "unstirred water layer" or to enable simulation of direct interactions between the compound of interest and the exterior cell membrane components. We can also anticipate a need to represent two or more different transporters by including objects similar to PGP within *G2* or *G4*. For example, objects representing apical uptake transporters, such as PEPT1 (peptide uptake transporter 1) and OCTN2 (Organic Cation Transporter 2), or additional efflux transporters, such as MRP2 (also known as cMOAT, an organic anion transporter) and BCRP (Breast Cancer Resistance Protein) can become *G2* components. Objects representing basolateral uptake transporters, such as OCT1 (Organic Cation Transporter 1), and efflux transporters, such as MRP3 (Multi-Drug Related Protein 3) and MCT1 (Monocarboxylate Transporter 1), can become *G4* components. We also anticipate the need to represent more detail associated with different types of metabolism, along with issues of induction and inhibition. Studies need not be limited to just one DRUG. Questions related to drug interactions can be explored. Such additional functionality and detail can be added or removed without compromising the remaining ISTS functionality.

To account for a mechanism whereby compounds are believed to interact with specific subcellular components—lysosomes, DNA, RNA, etc.—it may be necessary to add new objects

to *G3* or replace that space with additional fine-grained spaces. An object representing CYP3A4 at one *G3* location can be replaced by an object acting as a container (29). The container may, for example, provide a virtual space occupied by representations of CYP3A4 along with representations of other metabolic enzymes. For example it may contain representations of Phase I enzymes, such as MAOs (the Monoamine Oxidase superfamily), and Phase II enzymes, such as UGTs (the UDP-Glucuronosyl Transferase superfamily) and members of the Sulfotransferase superfamily. Again, because of the modular, synthetic nature of ISTSs, additions, replacements, and substitutions can be made relatively easily and without compromising the functionality built into the other parts of the model. Replacing G3 with two or more different grids (of the same size) can be done so that it will not interfere with the functionality elsewhere in the ISTS; such replacements can be done while a simulation is running, for example to simulate the consequences of some treatment effect or a therapeutic intervention. After validation against *in vitro* data, as was done for alfentanil and digoxin (3), the ISTS and its components can be used in new ways. For example, the cellular ISTS component can be removed for reuse as a module in a larger model. Assume that we have a physiologically based synthetic model that can represent gastro-intestinal absorption, and that it has been designed so that a connected array of similar modules represents the intestinal epithelium. Copies of a validated ISTS module that has compatible interfaces can be plugged into that array. Following parameterization of the other components of the gastro-intestinal model, simulations would anticipate the absorption properties of the compounds for which the ISTS had been validated.

Flexibility and adaptability are basic characteristics of biological systems of all types. However, it is challenging to achieve such characteristics using continuous state, equation-based models. That distinction is one of several that make it attractive to use this new class of models to represent and study biological systems, and as adjutants to make costly wetlab or clinical experiments more effective. These distinctions are important. The components of multicompartment absorption models are mathematical compressions of the phenomena that they model. The inductive method on which they are based explicitly uses the observed phenomena (the data) as its input whereas the synthetic method *begins* with proposed building blocks and the relations between them (14, 15). The inductive method starts with the phenomena—the amount absorbed and metabolized after some time, for example—and works backward to the generators in an attempt to discover an *inverse* mapping from range to domain. The synthetic method, in contrast, works *forward* from domain (building blocks) to range (behavior). Its constraints and criteria sit primarily in the domain.

Induced models are ideally suited for exploiting discovered characteristics whereas synthetic models are ideally suited for exploring the consequences of assembled components. The inductive model will provide a better fit to the data and greater precision in extrapolating that data under the same experimental conditions. The synthetic model will provide a hypothesis for the mechanisms that are believed to generate the data. Through its design and the stochastic nature of its component interactions, it also provides an important representation of uncertainty. An inductive model allows one to falsify claims *about the data* (relative to a given model). The synthetic model allows one to falsify claims *about the mechanisms*. The fundamental difficulty with the synthetic method, as applied here, is establishing requirements for building an analog that functions acceptably like an intestine, a monolayer of epithelial cells, or some other system. Synthetic modeling requires knowledge of the function of the referent, of plausible mechanisms for that function, and of relevant observables by which the analog and the referent will be measured and compared. Today, in pharmaceutical research, those requirements can be met. Building the models requires rigorous methods and attention to detail. It is too early in the development of this new class of models, however, to be able to know which specific in silico methods and procedures will prove to be most useful and effective.

In summary, we have provided an example of synthetic modeling and simulation applied to a pharmaceutically relevant domain: the transport of compounds across complex cellular barriers

that are capable of diverting it, metabolizing it, and directly responding to it. The system used are analogs of the CYP3A4-transfected Caco-2 transwell system. Experiments conducted using these ISTSs convincingly demonstrate the feasibility and suggest that they could be further developed in order to become stand-alone experimental systems that, within a research and development environment, will complement their *in vitro* counterparts. We simulated and explored the combined influences of apical efflux by Pgp and metabolism by CYP3A4 on transport and ER for series of virtual compounds having different degrees of overlapping affinities for Pgp and CYP3A4. We found that for dual substrates, system level transport properties were different with and without the spatial alignment of those components. In some cases, the efflux and metabolism influences were simply additive. However, for greater component density and for longer experiments, significant synergy was observed.

ACKNOWLEDGEMENTS

This research was funded in part by the CDH Research Foundation (R21-CDH-00101). We thank the members of the Biosystems Group for helpful discussion and commentary, with special thanks going to Jesse Engelberg, Pearl Johnson, Sean Kim, Tai Ning Lam, Glen Ropella, Amina Qutub, Jon Tang, and Betty-ann Hoener.

Abbreviations: A: apical; ANOVA: analysis of variance; B: basolateral; CYP: the in silico counterpart to CYP3A4; ER: extraction ratio; ISTS: in silico transwell system; Pgp: P-glycoprotein; PGP: the in silico counterpart to P-glycoprotein.

REFERENCES

1. L. Z. Benet, C. L. Cummins, and C. Y. Wu. Unmasking the dynamic interplay between efflux transporters and metabolic enzymes. *Int J Pharm* **277**: 3-9 (2004).
2. G. M. Grass. Simulation models to predict oral drug absorption from in vitro data. *Advanced Drug Delivery Reviews* **23**: 199-219 (1997).
3. Y. Liu, and C. A. Hunt. Studies of intestinal drug transport using an in silico epithelio-mimetic device. *Biosystems* **in press**: (2005).
4. V. J. Wacher, L. Salphati, and L. Z. Benet. Active secretion and enterocytic drug metabolism barriers to drug absorption. *Adv Drug Deliv Rev* **46**: 89-102 (2001).
5. V. J. Wacher, C. Y. Wu, and L. Z. Benet. Overlapping substrate specificities and tissue distribution of cytochrome P450 3A and P-glycoprotein: implications for drug delivery and activity in cancer chemotherapy. *Mol Carcinog* **13**: 129-34 (1995).
6. E. G. Schuetz, W. T. Beck, and J. D. Schuetz. Modulators and substrates of P-glycoprotein and cytochrome P4503A coordinately up-regulate these proteins in human colon carcinoma cells. *Mol Pharmacol* **49**: 311-8 (1996).
7. K. T. Kivisto, M. Niemi, and M. F. Fromm. Functional interaction of intestinal CYP3A4 and P-glycoprotein. *Fundam Clin Pharmacol* **18**: 621-6 (2004).
8. E. Wang, K. Lew, M. Barecki, C. N. Casciano, R. P. Clement, and W. W. Johnson. Quantitative distinctions of active site molecular recognition by P-glycoprotein and cytochrome P450 3A4. *Chem Res Toxicol* **14**: 1596-603 (2001).
9. K. Ito, H. Kusuhara, and Y. Sugiyama. Effects of intestinal CYP3A4 and P-glycoprotein on oral drug absorption--theoretical approach. *Pharm Res* **16**: 225-31 (1999).
10. P. B. Watkins. The barrier function of CYP3A4 and P-glycoprotein in the small bowel. *Adv Drug Deliv Rev* **27**: 161-170 (1997).
11. J. H. Hochman, M. Chiba, J. Nishime, M. Yamazaki, and J. H. Lin. Influence of P-glycoprotein on the transport and metabolism of indinavir in Caco-2 cells expressing cytochrome P-450 3A4. *J Pharmacol Exp Ther* **292**: 310-8 (2000).

12. P. Schmiedlin-Ren, K. E. Thummel, J. M. Fisher, M. F. Paine, K. S. Lown, and P. B. Watkins. Expression of enzymatically active CYP3A4 by Caco-2 cells grown on extracellular matrix-coated permeable supports in the presence of 1alpha,25-dihydroxyvitamin D3. *Mol Pharmacol* **51**: 741-54 (1997).
13. C. L. Crespi, B. W. Penman, and M. Hu. Development of Caco-2 cells expressing high levels of cDNA-derived cytochrome P4503A4. *Pharm Res* **13**: 1635-41 (1996).
14. G. E. P. Ropella, C. A. Hunt, and S. Sheikh-Bahaei. Methodological considerations of heuristic modeling of biological systems, *The 9th World Multi-Conference on Systemics, Cybernetics and Informatics*, Orlando, FL, 2005.
15. G. E. P. Ropella, C. A. Hunt, and D. A. Nag. Using heuristic models to bridge the gap between analytic and experimental models in biology, *SpringSim'05*, San Diego, CA, 2005.
16. N. Gilbert, and S. Bankes. Platforms and methods for agent-based modeling. *Proc Natl Acad Sci U S A* **99 Suppl 3**: 7197-8 (2002).
17. A. Walter, and J. Gutknecht. Permeability of small nonelectrolytes through lipid bilayer membranes. *J Membr Biol* **90**: 207-17 (1986).
18. T. X. Xiang, and B. D. Anderson. Diffusion of ionizable solutes across planar lipid bilayer membranes: boundary-layer pH gradients and the effect of buffers. *Pharm Res* **10**: 1654-61 (1993).
19. C. L. Cummins, L. M. Mangravite, and L. Z. Benet. Characterizing the expression of CYP3A4 and efflux transporters (P-gp, MRP1, and MRP2) in CYP3A4-transfected Caco-2 cells after induction with sodium butyrate and the phorbol ester 12-O-tetradecanoylphorbol-13-acetate. *Pharm Res* **18**: 1102-9 (2001).
20. L. Steels, and R. Brooks. The Artificial Life Route to Artificial Intelligence: Building Embodied, Situated Agents, Lawrence Earlbaum Associates, Hillsdale, NJ (1995).
21. M. E. Andersen. Toxicokinetic modeling and its applications in chemical risk assessment. *Toxicol Lett* **138**: 9-27 (2003).
22. D. Noble. The rise of computational biology. *Nat Rev Mol Cell Biol* **3**: 459-63 (2002).
23. H. Kitano. Computational systems biology. *Nature* **420**: 206-210 (2002).
24. L. Z. Benet, and C. L. Cummins. The drug efflux-metabolism alliance: biochemical aspects. *Adv Drug Deliv Rev* **50 Suppl 1**: S3-11 (2001).
25. S. J. Mouly, M. F. Paine, and P. B. Watkins. Contributions of CYP3A4, P-glycoprotein, and serum protein binding to the intestinal first-pass extraction of saquinavir. *J Pharmacol Exp Ther* **308**: 941-8 (2004).
26. J. H. Hochman, M. Chiba, M. Yamazaki, C. Tang, and J. H. Lin. P-glycoprotein-mediated efflux of indinavir metabolites in Caco-2 cells expressing cytochrome P450 3A4. *J Pharmacol Exp Ther* **298**: 323-30 (2001).
27. M. F. Paine, L. Y. Leung, H. K. Lim, K. Liao, A. Oganesian, M. Y. Zhang, K. E. Thummel, and P. B. Watkins. Identification of a novel route of extraction of sirolimus in human small intestine: roles of metabolism and secretion. *J Pharmacol Exp Ther* **301**: 174-86 (2002).
28. C. L. Cummins, W. Jacobsen, and L. Z. Benet. Unmasking the dynamic interplay between intestinal P-glycoprotein and CYP3A4. *J Pharmacol Exp Ther* **300**: 1036-45 (2002).
29. B. P. Zeigler. *Objects and Systems: Principled Design with Implementations in C++ and Java*, Springer-Verlag, New York, 1997.

Tables

Table I. Binding affinities of CYP and PGP for the hypothetical drugs[1]

DRUG ID	*cypSoluteAffinity* [2]	*pgpSoluteAffinity* [2]	DRUG ID	*cypSoluteAffinity* [2]	*pgpSoluteAffinity* [2]
I	0	0	**IX**	0.75	0
II	0	0.5	**X**	0.75	0.5
III	0	0.75	**XI**	0.75	0.75
IV	0	1.0	**XII**	0.75	1.0
V	0.5	0	**XIII**	1.0	0
VI	0.5	0.5	**XIV**	1.0	0.5
VII	0.5	0.75	**XV**	1.0	0.75
VIII	0.5	1.0	**XVI**	1.0	1.0
			XVII [3]	0.5	0.5

[1] Each DRUG is a weak base with $pK_a = 6.5$. [2] Binding is a probabilistic event; if the affinity value is high, e.g., 0.75, then when substrate is next to the active site, there is a 75% chance (on average) that it will be bound at the next time step. [3] **XVII** has MW of 300 Daltons and *logP* of 1.8; all other DRUGS have MW of 150 Daltons and *logP* of 2.0

Table II. Parameters[1] of the ISTS

Category	Name	Description	Values
In silico Transwell System	*worldXSize* *worldYSize*	The X x Y dimension of *G1 – G5*	100 x 100 [2]
	tightJunctions	Tight junction area as % MEMBRANE space area	0.1
	minPgps	Minimum PGP density	10
	maxPgps	Maximum PGP density	50
	minCyps	Minimum CYP density	20
	maxCyps	Maximum CYP density	50
DRUG Properties	*ionDiffusion*	Permeation due to ionized form of DRUG (%)	0 ~ 1
	substrateOfPgp	DRUG is a substrate of PGP or not	T or F
	pgpSoluteAffinity	DRUG–PGP binding affinity	0 ~ 1.0
	substrateOfCyp	DRUG is a substrate of CYP or not	T or F
	cypSoluteAffinity	DRUG–CYP binding affinity	0 ~ 1.0
Exp. Conditions	*numSolutes*	Initial concentration in donor compartment	2000
	a2bDirection	Donor is *G1* (otherwise, *G5*)	T or F

[1] The ISTS contains additional parameters (3) that were not adjusted during the experiments discussed herein or in related exploratory experiments. Examples include parameters to adjust molecular weight, pK_a, logarithm of the (DRUG'S) partition coefficient, pH in *G1, G3,* and *G5*. [2] This grid size was adequate for the needs of this study; it can be changed easily thereby altering system resolution.

Table III. Comparison of the efflux ratios[1] and the influence of inhibition of PGP on the extent of metabolism for four hypothetical DRUGS

Drug	Efflux ratio	ER (S.D.)[2]		Δ
	B→A / A→B	DRUG alone	Inhibit PGP	%
VI	1.423	0.170 (0.017)	0.164 (0.015)	3.5
XVII	2.584	0.454 (0.028)	0.389 (0.026)	14.3
VIII	1.602	0.179 (0.014)	0.164 (0.015)	8.4
XIV	1.446	0.242 (0.030)	0.216 (0.025)	11

[1] Measured under a sink condition. [2] Data are shown as mean (S.D.) from 10 Monte Carlo simulations

Table IV. The combined influences of CYP and PGP on the simulated absorption (A→B transport) of DRUGS **VI** and **XI**

	ISTS (20 CYPs, 30 PGPs)		ISTS (50 CYPs, 50 PGPs)	
	Ab %[1]	Δ (%)[2]	Ab %	Δ (%)
Control (**VI** @ 800)	8.23		6.24	
Inhibit PGP	9.99	1.76	8.16	1.92
Inhibit CYP	9.66	1.43	8.36	2.12
Expected (E) upon inhibition of both[3]	11.42	3.19	10.28	4.04
Observed (O) upon inhibition of both	11.30	3.07	11.30	5.06
Synergism: O/E (**VI** @ 800)	0.99	0.96	1.10	1.25
Synergism: O/E (**XI** @ 800) [4]	1.04	1.15	1.21	1.53
Synergism: O/E (**XI** @ 400) [4]	0.96	0.83	1.03	1.09

[1] Percent ABSORBED (in *G5* at time step 800, for **VI** and **XI**, and at time step 400 for **XI**); data are shown as mean from 10 Monte Carlo simulations; [2]Additional ABSORPTION relative to control values; [3]Assuming effects are additive. [4] Calculated as for **VI**.

Table V. ANOVA[1] table for testing the competitive inhibitory effect of METABOLITES on the DRUG flux rate (sink conditions)

	A→B					B→A				
	DF	Sum of Sq.	Mean Sq.	F-value	Pr (F)	DF	Sum of Sq.	Mean Sq.	F-value	Pr (F)
Hypothetical DRUGS	15	0.45	0.030	238.28	0	15	1.07	0.071	243.62	0
Mechanism	1	5.90E-05	5.90E-05	0.47	0.49	1	6.28E-06	6.28E-06	0.021	0.88
Two terms interaction	15	9.44E-04	6.29E-05	0.50	0.94	15	0.0013	8.61E-05	0.29	0.99
Residuals	288	0.036	1.26E-04			288	0.084	2.92E-04		

[1] The ANOVA model is Flux Rate = DRUG + Mechanism + (DRUG x Mechanism) + residual.

Table VI. ANOVA[1] table for testing the competitive inhibitory effect of METABOLITES on the DRUG ER (sink conditions)

	A→B					B→A				
	DF	Sum of Sq.	Mean Sq.	F-value	Pr (F)	DF	Sum of Sq.	Mean Sq.	F-value	Pr (F)
Hypothetical DRUGS	15	12.57	0.84	1332.6	0	15	7.09	0.47	924.91	0
Mechanism	1	2.47E-04	2.47E-04	0.39	0.53	1	3.07E-04	3.07E-04	0.60	0.44
Two terms interaction	15	0.0068	4.55E-04	0.72	0.76	15	0.0096	6.39E-04	1.25	0.23
Residuals	288	0.18	6.29E-04			288	0.15	5.11E-04		

[1] The ANOVA model is ER = DRUG + Mechanism + (DRUG x Mechanism) + residual.

Figures Captions

Studies of Transport Using the Synthetic Method Pharm. Resh. PMID: 16435171

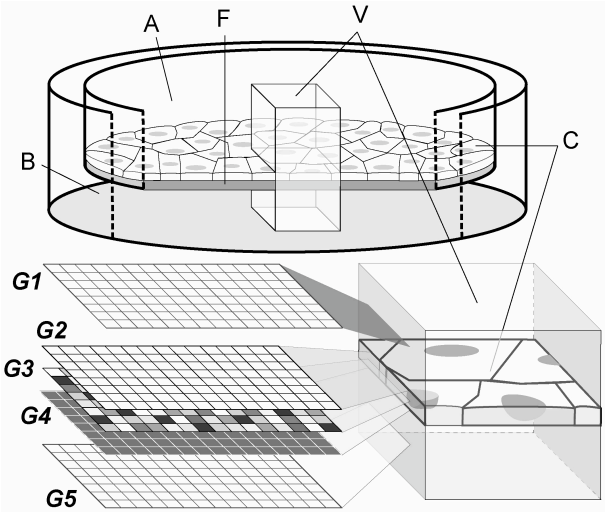

Fig. 1. *In vitro* and in silico experimental system to study intestinal drug transport and metabolism. CYP3A4-transfected Caco-2 *in vitro* transwell system: A: apical, B: basolateral compartment; C: epithelial cell monolayer; F: filter; V: a vertical column section through the transwell system. In silico transwell system (ISTS): *G1–G5*: 2D grid spaces representing the indicated components of the transwell system. The different shading of the *G3* grid locations illustrates that locations in any of the five spaces can have different properties (see the text for additional detail).

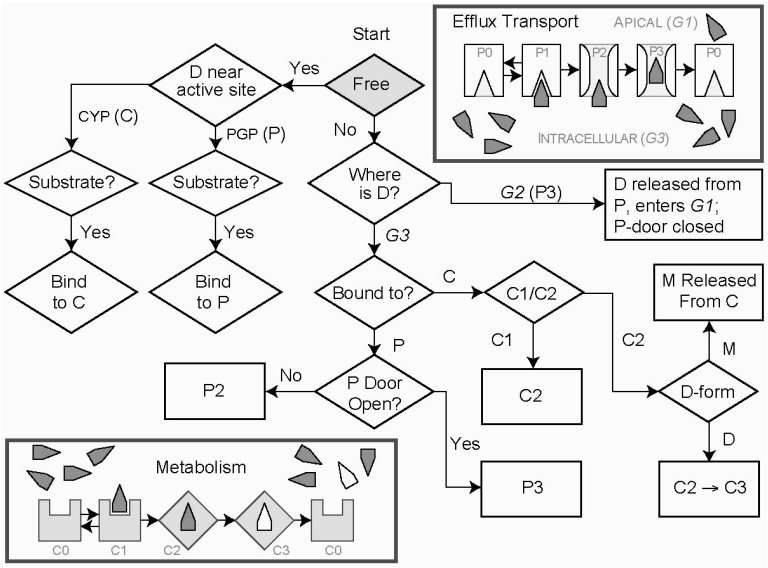

Fig. 2. A flowchart describing the ISTS efflux transport and METABOLISM processes. D: a DRUG object; P: a PGP object; C: a CYP object. The algorithm is designed according to the schematics in the inserts. Inserts: gray objects represent DRUG; white objects represent METABOLITE; notched and open white boxes: different PGP states; notched and diamond-shaped gray boxes: different CYP states. Binding between P or C, and D is probabilistic and is controlled by the simulation parameters *pgpSoluteAffinity*, *cypSoluteAffinity* respectively.

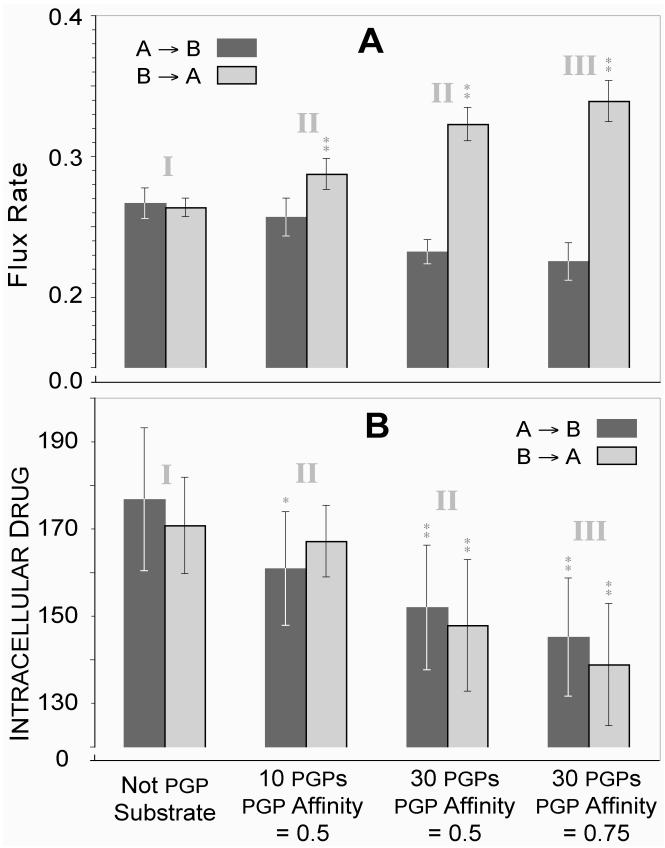

Fig. 3. Effect of PGP on flux rates and simulated intracellular DRUG levels for **I**, **II**, and **III**. (A) Simulated transepithelial flux rate of **I**, **II**, and **III** under a sink condition; A→B transport measures serve as controls. (B) Dark gray bars: simulated intracellular DRUG levels at time step 400 following dosing into *G1*; light gray bars: simulated intracellular DRUG levels at time step 400 following dosing into *G5*; the data from **I** (not PGP substrate) served as controls. ∗: difference between experimental and control groups is significant ($p < 0.05$); ∗∗: difference between experimental and control groups is highly significant ($p < 0.01$); the Welch modified two-sample *t*-test was used. Data are the mean of 10 Monte Carlo simulations; error bars: ± S.D.

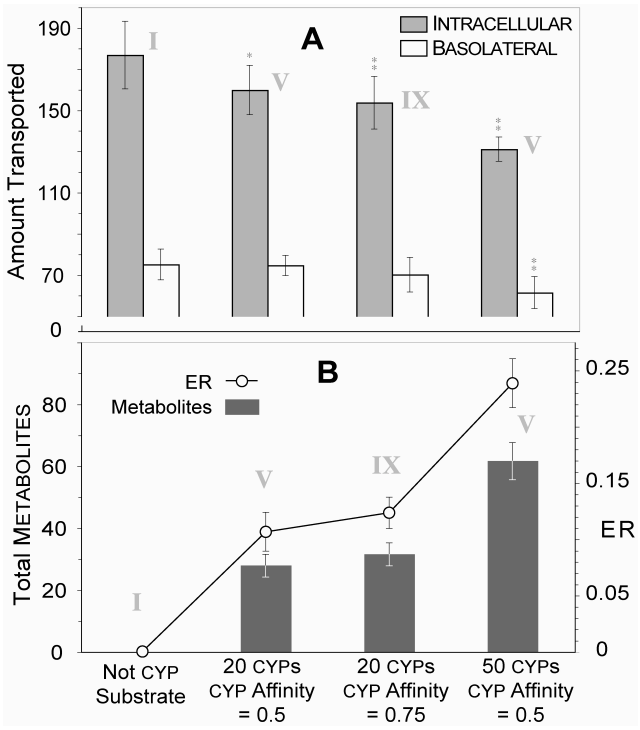

Fig. 4. Effect of CYP on simulated A→B transepithelial transport and the extent of METABOLISM for **I**, **V**, and **IX**. (A) Amounts of DRUG found in simulated cells and transported to the simulated basolateral compartment (*G5*) were measured at time step 400. The data from **I** (not CYP substrate) served as controls. (B) Simulated CYP-mediated metabolism, as measured by the formation of METABOLITES and the calculated ER. Sample size, ∗, and ∗∗: as in Fig. 3.

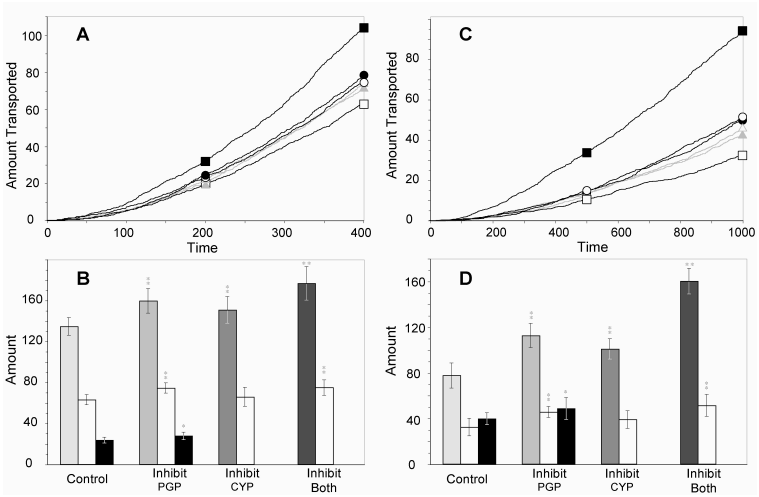

Fig. 5. The influence of PGP and CYP (and their inhibition) on simulated transcellular transport (A and C) and formation of METABOLITES (B and D) for dual substrates **VI** (A and B at time step 400) and **XVII** (C and D at time step 1000; because of the physicochemical properties of **XVII**, a longer study period was required to get amounts similar to those for **VI**). (A, C) Each line is composed of mean measurements taken at each time step. Symbols are added to differentiate the six curves. Open symbols: A→B transport; closed symbols: B→A transport; squares: controls (no inhibition of either PGP or CYP); triangles: complete inhibition of PGP; circles: complete inhibition of PGP and CYP. Inserts are two enlarged illustrations for a short time interval. (B, D) Gray bars: simulated cellular DRUG levels; open bars: *G5* (simulated basolateral) DRUG levels; dark bars: total METABOLITES in all spaces. Sample size, ∗, and ∗∗: as in Fig. 3.

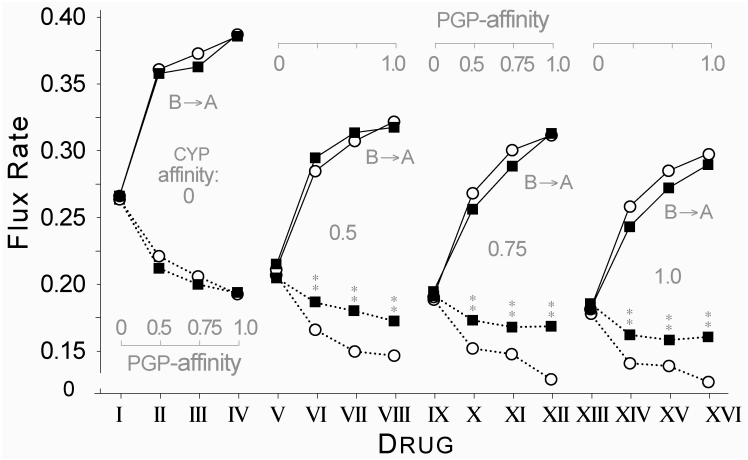

Fig. 6. The influence of the relative positioning of PGP and CYP on flux rates of **I–XVI**. Each set of experiments used the same ISTS (50 PGP, 50 CYP). Experiments are clustered into four groups based on CYP-DRUG affinity. Within each group, the inserted scale shows PGP-DRUG affinity. Open circles: mean of control experiments (the locations of PGP and CYP within *G2* and *G3*, respectively, are uncorrelated); closed squares: mean of experimental group (the locations of PGP and CYP within *G2* and *G3* are matched); dashed line: A→B transport; solid line B→A transport. Sample size, ∗, and ∗∗: as in Fig. 3.

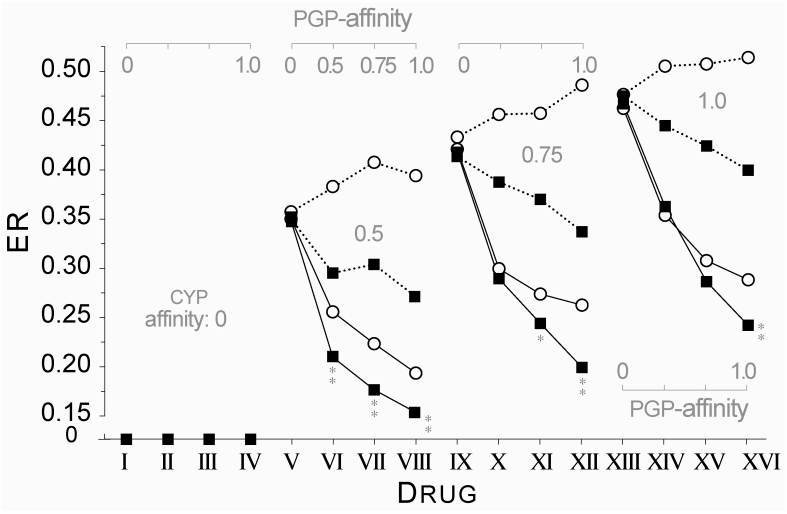

Fig. 7. The influence of the relative positioning of PGP and CYP on ER of I–XVI. The representations and details are the same as in Fig. 6.